ISSN 1990-7931, Russian Journal of Physical Chemistry B, 2025, Vol. 19, No. 4, pp. 943–952. © Pleiades Publishing, Ltd., 2025.

CHEMICAL PHYSICS OF NANOMATERIALS

Monotiring of Zinc Oxide and Zinc Sulfide-Based as Smart Nanomaterials for Water Treatment Through Electron Transfer Characteristics and Density of States Analysis: A Quantum Chemistry Study

F. Mollaamin[a], * and M. Monajjemi[b]

[a] *Department of Biomedical Engineering, Faculty of Engineering and Architecture, Kastamonu University, Kastamonu, Turkey*
[b] *Department of Chemical Engineering, Central Tehran Branch, Islamic Azad University, Tehran, Iran*
**e-mail: fmollaamin@kastamonu.edu.tr*

Received February 13, 2025; revised April 14, 2025; accepted April 21, 2025

Abstract—The world encounters an increasing challenge for adequate clean water owing to threats coming from enhancing request and reducing supply. In nanoscale, zinc oxide and zinc sulfide have indicated antimicrobial properties which make its potential great for different applications. We employ first-principles calculations to investigate the structural stability and electronic properties of cubic zinc oxide (ZnO) and zinc sulfide (ZnS) heteroclusters with H_2O molecules adsorbed on them. A comprehensive investigation on H_2O grabbing by ZnO/ZnS heteroclusters was carried out using density functional theory (DFT) computations at the Coulomb-attenuating method–Becke, 3-parameter, Lee–Yang–Parr with Dispersion–corrected (CAM–B3LYP–D3/6–311+G(*d*, *p*)) level of theory. The notable fragile signal intensity close to the parallel edge of the nanocluster sample might be owing to H/OH binding induced non-spherical distribution of ZnO or ZnS heterocluster. The hypothesis of the energy adsorption phenomenon was confirmed by density distributions of charge density differences, total density of states and molecular electrostatic potential for ZnO/ZnO(H_2O) or ZnS/ZnS(H_2O). A vaster jointed area engaged by an isosurface map for H/OH adsorption on ZnO or ZnS surface towards formation of ZnO(H_2O) or ZnS(H_2O) complex. Therefore, it can be considered that zinc in the functionalized ZnO or ZnS might have more impressive sensitivity for accepting the electrons in the process of H/OH adsorption. It is considerable that when all surface atoms of ZnO or ZnS are coated by OH and H groups, the semiconducting behavior is recovered.

Keywords: ZnO/ZnO(H_2O), ZnS/ZnS(H_2O), semiconductor, H/OH adsorption, density of states
DOI: 10.1134/S1990793125700605

1. INTRODUCTION

Zinc oxide (ZnO) is a promising semiconductor material for various applications ranging from optoelectronics to biomedicine, attributed to its wide direct band gap, high exciton binding energy, high mobility, and high quantum efficiency. To further improve the performance of ZnO devices, plasma treatment is a common method for surface modification [1–4]. The luminescence properties of ZnO after plasma treatment are significantly changed, including ultraviolet (UV) luminescence, visible luminescence, and recombination mechanism [5–11].

Optical properties are improved significantly by H plasma, with negligible alteration in thickness. Although no chemical reaction is introduced, emission intensity is enhanced by Ar plasma by eliminating the non-radiative recombination centers. Furthermore, H and Ar plasma also induce strong exciton localization, leading to significant broadening of the UV spectrum [12–15]. However, replicating or applying the reported improvement in plasma treatments for ZnO often proves challenging. This difficulty arises from several factors, including the diverse properties of ZnO samples, which encompass thin films, single crystals and nanostructures grown through various methods. Moreover, the specific effects of plasma treatments using different gases remain unclear, as each type of gas plasma exhibits unique interactions. Consequently, it is crucial to conduct a systematic comparison of the influence of various plasma gases on the optical and electrical properties and to accurately identify the specific defects affected [16–21].

Transparent, superhydrophilic materials are indispensable for their self-cleaning function, which has become an increasingly popular research topic, particularly in photovoltaic (PV) applications. It was reported hydrophilic and superhydrophilic ZnO by varying the morphology for use as a self-cleaning coat-

ing for PV applications [22]. The researchers have applied molecular dynamics simulations through a reactive force-field for ZnO–H_2O ambient. The force-field parameters were fitted to a dataset of energies, geometries and charges derived from density functional theory calculations. The applied model has provided a good fit to the quantum mechanics reference data for the ZnO–H_2O system that was present in the dataset. The force-field has been used to study how H_2O is adsorbed, molecularly or dissociatively, at monolayer coverage on flat and stepped ZnO surfaces, at different temperatures. The results show that structures that promote hydrogen bonding are favored, and that the presence of steps promotes an increased level of hydroxylation in the water monolayers [23].

The cubic form of zinc sulfide (ZnS) is the prototype II–VI semiconductor with smallest lattice constant of $a_0 = 5.4102$ Å at 300 K and the primarily candidate for UV-light emitting devices because of its large band-gap energy around ~3.7 eV at room temperature [24, 25]. Many research groups have attempted to dope anions and cations into the ZnO or ZnS lattice, which helps to reach various complex applications since its electronic structure and characteristics may be significantly adjusted. The enhanced catalytic properties reveal the synergy between ZnO and ZnS functional nanomaterials, which upgrade the electron-hole pair, resulting in enhanced catalytic performance under the visible region. Notably, the ZnO-based ZnS nanocomposite was prepared by a wet chemical method without any template [26–29]. The template method is not sensitive to the preparation conditions, is easy to operate and implement, and controls nanomaterials' structure, morphology, and particle size through the template material. Generally, the outstanding photocatalytic performance of wurtzite ZnO and ZnS semiconductor and their composite under visible light irradiation could be attributed to synergistic effects when coupled with other metal oxide semiconductor. The present study is a part of our ongoing research to understand the solar energy conversion/harvesting directions. We reported a facile synthesis of ZnS and ZnO nanoparticles and their nanocomposites by the wet chemical method [30–34]. In this work, we analyzed the effect of H_2O adsorption on the properties of ZnO or ZnS heterocluster via the density of state, charge distribution, bond orders and HOMO–LUMO orbitals using DFT studies.

2. THEORY, MATERIALS AND COMPUTATION

The process of hydration for ZnO or ZnS and formation of ZnO(H_2O) or ZnS(H_2O) heterocluster was calculated within the framework of first-principles calculation based on density functional theory (DFT) (Figs. 1a, 1a', 1b, 1b'). The rigid potential energy surface using density functional theory [35–48] was performed due to Gaussian 16 revision C.01 program package [49] and GaussView 6.1 [50]. The coordination input for energy storage on the solar cells has applied 6–311+G(d, p) and EPR–3 basis sets [51, 52].

First, we optimized the structural parameters of the nanocluster of ZnO or ZnS and hydrated nanocluster of ZnO(H_2O) or ZnS(H_2O) for obtaining the highest short-circuit current density. Figures 1a, 1a', 1b, 1b' shows the process of H_2O-adsorption on nanocluster of ZnO or ZnS which is varied to maximize the absorption in the active region. This is a utility used to calculate ring area and perimeter, since ring area is sometimes involved in wavefunction analysis. In this function, it is needed to input the index of the atoms in the ring in clockwise manner which can conclude the total ring area and total ring perimeter for a tailored ring as 9.4242 Å and 12.2796 Å^2 for ZnO (Fig. 1a) and 9.4240 Å and 12.2794 Å^2 for ZnS, respectively (Fig. 1b).

3. RESULTS AND DISCUSSION

Notwithstanding the many areas to be explored further, the outlook of progressing intense and diverse research on ZnO or ZnS is evidence of its potential as a water disinfectant at the industrial level. In this article, the data has evaluated the efficiency of ZnO or ZnS in H_2O medium through energies, geometries and charges derived from density functional theory calculations. The applied model has provided a good fit to the quantum mechanics reference data for the ZnO(H_2O) or ZnS(H_2O) systems that was present in the dataset. The force-field has been used to study how water is adsorbed, molecularly at monolayer coverage on ZnO or ZnS surfaces.

The amounts of charge density differences (CDD) [53] are measured by considering isolated atoms or noninteracting ones. The mentioned approximation can be the lightest to use because the superposition value may be received from the primary status of the self-consistency cycle in the code that carries out the density functional theory (Figs. 2a, 2a', 2b, 2b') [46]. Figures 2a, 2b indicates all Zn, O or S atoms of ZnO or ZnS fluctuating around –9 to –1 Bohr. In Figs. 2a', 2b', the atom of Zn15, O27 or S27 from ZnO(H_2O) or ZnS(H_2O) and O1, H29, H30 from H_2O molecule accompanying other Zn, O or S atoms from ZnO(H_2O) or ZnS(H_2O) have shown the fluctuation around –1 to +1 Bohr and –9 to +1 Bohr, respectively.

Furthermore, atomic charge was discussed during H_2O adsorption by ZnO or ZnS towards formation of ZnO(H_2O) or ZnS(H_2O) (Table 1). The atomic charge of Zn, O or S, and H/OH adsorbed on ZnO or ZnS have been measured. The values detect that with adding H_2O, the negative atomic charge of oxygen atoms of O16, O17, O18, O19, O20, O21, O22, O23, O24, O25, O26, O27, O28 in ZnO(H_2O) has changed through coating of ZnO with H/OH. In fact, ZnO(H_2O) has shown more efficiency than ZnO for

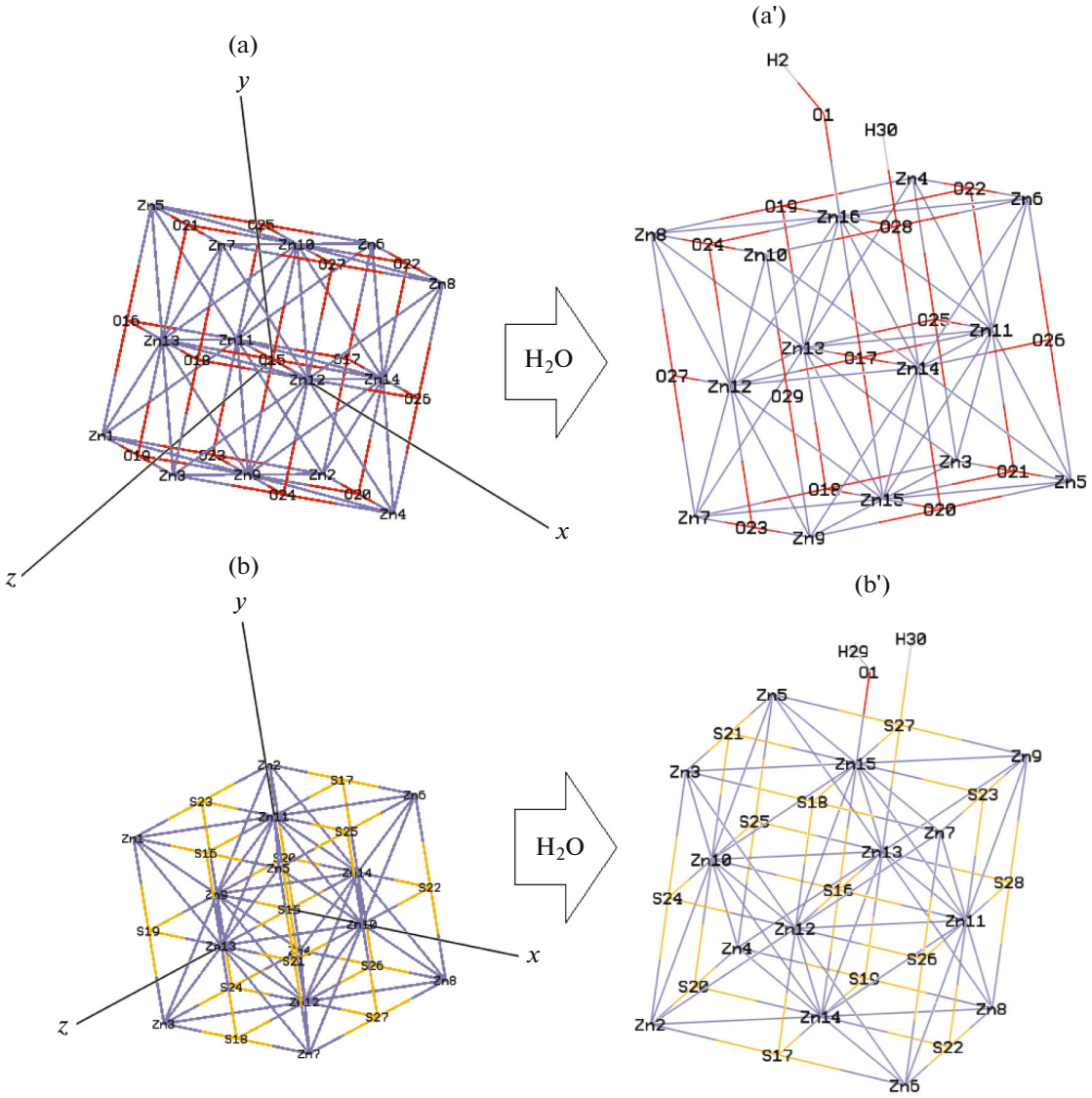

Fig. 1. Characterization of (a) ZnO/ ZnO(H_2O) and (b) ZnS/ ZnS(H_2O) heteroclusters including H, O, S, Zn atoms towards H_2O-adsorption.

admitting the electron from electron donor of O16 to O28 (Table 1 and Figs. 3a, 3a'). However, the negative atomic charge of zinc atoms and loss of negative atomic charge of sulfur in ZnS/ZnS(H_2O) have been observed through Table 1 and Figs. 3b, 3b'. The changes of charge density analysis in the adsorption process have illustrated that ZnO and ZnO(H_2O) nanoclusters have shown the Bader charge of −1.747 and −1.900 coulomb, respectively. The differences of charge density for these structures are measured as: $\Delta Q_{\text{ads. ZnO(H2O)}} = -0.153$ coulomb [54]. The changes of charge density analysis in the adsorption process have illustrated that ZnS and ZnS(H_2O) nanoclusters have shown the "Bader charge" of −0.670 and −2.667 coulomb, respectively. The differences of charge density for these structures are measured as: $\Delta Q_{\text{ads. ZnS(H2O)}} = -1.997$coulomb.

To better understand the different adsorption characteristics of ZnO/ZnO(H_2O) and ZnS/ZnS(H_2O) heteroclusters, total density of states (TDOS) using Multiwfn program [55, 56] has been measured. This parameter can indicate the existence of important chemical interactions often on the convex side (Figs. 4a, 4a', 4b, 4b'). In an isolated system (such as molecule), the energy levels are discrete, the concept of density of state (DOS) is supposed to be completely valueless in this situation. Therefore, the original total DOS (TDOS) of the isolated system can be written as [57]:

$$\mathrm{TDOS}(E) = \sum_i \delta(E - \epsilon_i), \tag{1}$$

$$G(x) = \frac{1}{c\sqrt{2\pi}} e^{-\frac{x^2}{2c^2}}, \text{ where } c = \frac{\mathrm{FWHM}}{2\sqrt{2\ln x}}. \tag{2}$$

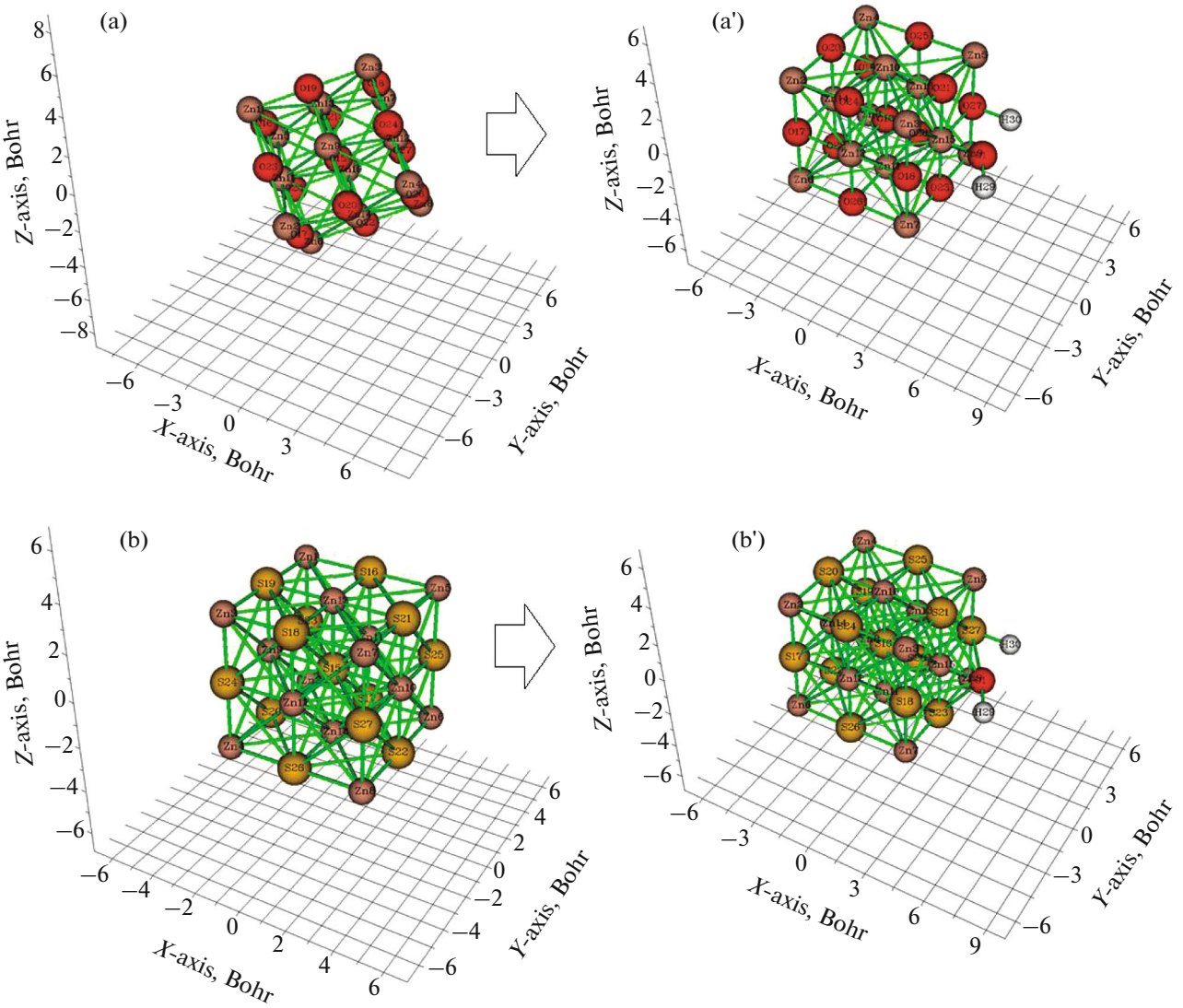

Fig. 2. CDD graphs for heteroclusters of (a) ZnO, (a') ZnO(H_2O), (b) ZnS, and (b') ZnS(H_2O).

Moreover, the curve map of broadened partial DOS (PDOS) and overlap DOS (OPDOS) are valuable for visualizing orbital composition analysis, PDOS function of fragment A is defined as:

$$\mathrm{PDOS}_A(E) = \sum_i \Xi_{i,A} F(E - \epsilon_i), \quad (3)$$

where $\Xi_{i,A}$ is the composition of fragment A in orbital i. The OPDOS between fragment A and B is defined as:

$$\mathrm{OPDOS}_{A,B}(E) = \sum_i X^i_{A,B} F(E - \epsilon_i), \quad (4)$$

where $X^i_{A,B}$ is the composition of total cross term between fragment A and B in orbital i. In the TDOS map, each discrete vertical line corresponds to a molecular orbital (MO), the dashed line highlights the position of HOMO. The curve is the TDOS simulated based on the distribution of MO energy levels. In the negative part, the region around −0.60 to −0.80 a.u. has obviously larger state density than other regions for ZnO and ZnO(H_2O) nanoclusters (Figs. 4a, 4a'). However, it has been shown a larger state density through pointed peaks for ZnO(H_2O) (Fig. 4a') than ZnO (Fig. 4a) around −0.20 to −0.40 a.u. It is remarkable that when all surface atoms of ZnO are coated by OH and H groups, the semiconducting behavior is recovered. Our results open up the possibility of tailoring the electronic properties by controlling the surface adsorption sites. In the positive part, the region around 0.1–0.2 a.u. has obviously larger state density than other regions for ZnS and ZnS(H_2O) nanoclusters (Figs. 4b, 4b').

Fragment 1 has been defined for Zn1 (Fig. 4a), O1 (Fig. 4a') and Zn2, Zn4, Zn6, Zn8, Zn10, O16, O19, O22, O24 (Figs. 4a, 4a') and H30 (Fig. 4a').

Table 1. The atomic charge (Q/coulomb) for heteroclusters of ZnO and ZnS through H/OH adsorption and formation of $ZnO(H_2O)$ and $ZnS(H_2O)$ heteroclusters

ZnO		$ZnO(H_2O)$		ZnS		$ZnS(H_2O)$	
atom	charge	atom	charge	atom	charge	atom	charge
Zn1	0.71	O1	−0.59	Zn1	−0.59	O1	−0.65
Zn2	0.71	Zn2	0.69	Zn2	−0.59	Zn2	−0.57
Zn3	0.71	Zn3	0.73	Zn3	−0.59	Zn3	−0.54
Zn4	0.71	Zn4	0.72	Zn4	−0.59	Zn4	−0.55
Zn5	0.71	Zn5	0.59	Zn5	−0.59	Zn5	−0.47
Zn6	0.71	Zn6	0.69	Zn6	−0.59	Zn6	−0.57
Zn7	0.71	Zn7	0.71	Zn7	−0.59	Zn7	−0.56
Zn8	0.71	Zn8	0.72	Zn8	−0.59	Zn8	−0.55
Zn9	1.74	Zn9	0.60	Zn9	−0.41	Zn9	−0.47
Zn10	1.74	Zn10	1.72	Zn10	−0.42	Zn10	−0.45
Zn11	1.74	Zn11	1.73	Zn11	−0.41	Zn11	−0.46
Zn12	1.74	Zn12	1.88	Zn12	−0.41	Zn12	−0.46
Zn13	1.74	Zn13	1.90	Zn13	−0.41	Zn13	−0.51
Zn14	1.74	Zn14	1.70	Zn14	−0.41	Zn14	−0.34
O15	−1.53	Zn15	1.48	S15	0.67	Zn15	−2.66
O16	−1.22	O16	−1.54	S16	0.54	S16	0.73
O17	−1.22	O17	−1.22	S17	0.54	S17	0.61
O18	−1.22	O18	−1.21	S18	0.54	S18	0.79
O19	−1.22	O19	−1.22	S19	0.54	S19	0.85
O20	−1.22	O20	−1.22	S20	0.54	S20	0.57
O21	−1.22	O21	−1.14	S21	0.54	S21	1.12
O22	−1.22	O22	−1.22	S22	0.54	S22	0.57
O23	−1.22	O23	−1.13	S23	0.54	S23	1.11
O24	−1.22	O24	−1.21	S24	0.54	S24	0.57
O25	−1.22	O25	−1.22	S25	0.54	S25	0.62
O26	−1.22	O26	−1.21	S26	0.54	S26	0.57
O27	−1.22	O27	−1.18	S27	0.54	S27	0.30
		O28	−1.22			S28	0.62
		H29	0.29			H29	0.46
		H30	0.37			H30	0.35

Moreover, Fragment 2 has indicated the fluctuation of Zn11, Zn12, Zn13, Zn14, O17, O25, O26, O27 for ZnO and $ZnO(H_2O)$ heteroclusters (Figs. 4a, 4a') and H29 for $ZnO(H_2O)$ (Fig. 4a'). Finally, it was considered the fluctuation of O15 (Fig. 4a), Zn15 (Fig. 4a') and Zn3, Zn5, Zn7, Zn9, O18, O20, O21, O23 for both ZnO and $ZnO(H_2O)$ nanoclusters (Figs. 4a, 4a') through Fragment 3. Moreover, Fragment 1 has been defined for Zn1 (Fig. 4b), O1 (Fig. 4b') and Zn2, Zn4, Zn6, Zn8, Zn10, S16, S19, S22, S24 (Figs. 4b, 4b') and H30 (Fig. 4b'). Moreover, Fragment 2 has indicated the fluctuation of Zn11, Zn12, Zn13, Zn14, S17, S25, S26, S27 for ZnS and $ZnS(H_2O)$ heteroclusters (Figs. 4b, 4b') and H29 for $ZnS(H_2O)$ (Fig. 4b'). Finally, it was considered the fluctuation of S15 (Fig. 4b), Zn15 (Fig. 4b') and Zn3, Zn5, Zn7, Zn9, S18, S20, S21, S23 for both ZnS and $ZnS(H_2O)$ heteroclusters (Figs. 4b, 4b') through Fragment 3.

This function measures the electrostatic interaction between a unit point charge placed at r and the system of interest. A positive (negative) value implies that the current position is dominated by nuclear (electronic) charges. Molecular electrostatic potential (ESP) has been widely used for prediction of nucleophilic and electrophilic sites for a long time. It is also valuable in studying hydrogen bonds, halogen bonds, molecular recognitions and the intermolecular interaction of aromatics [58–60]:

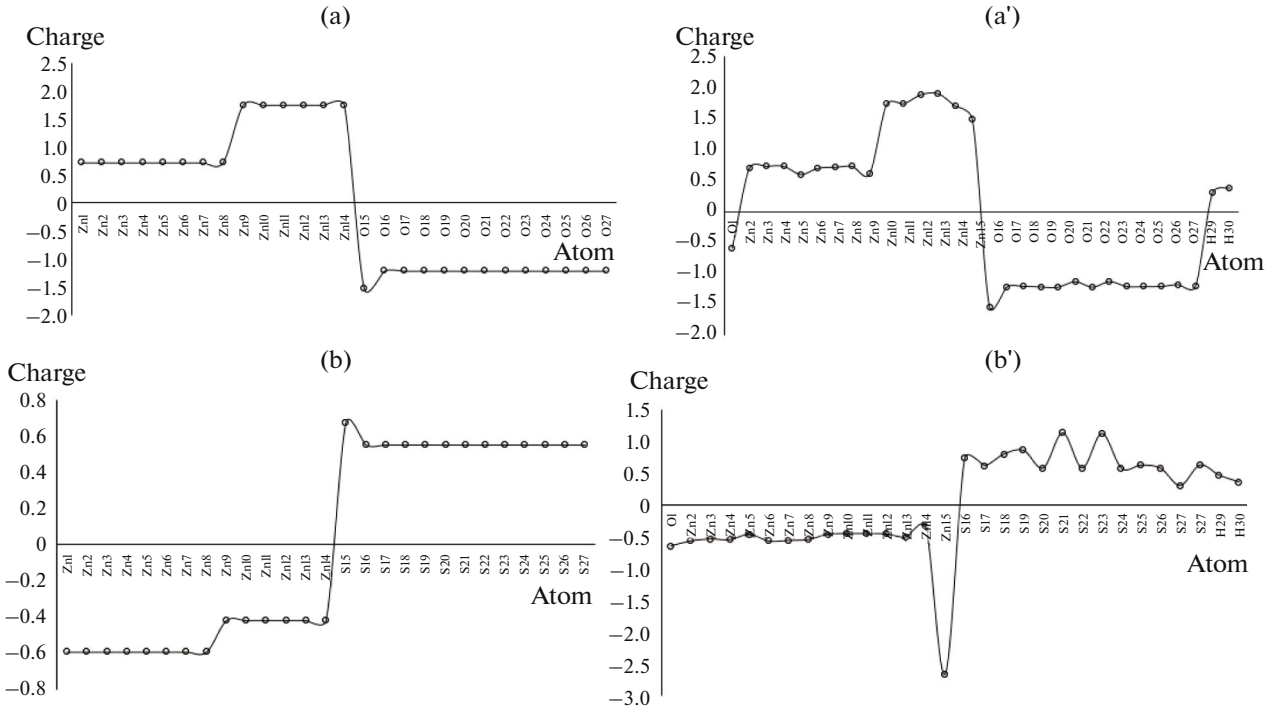

Fig. 3. The fluctuation of atomic charge (Q/coulomb) for (a) ZnO (a') $ZnO(H_2O)$, (b) ZnS and (b') $ZnS(H_2O)$.

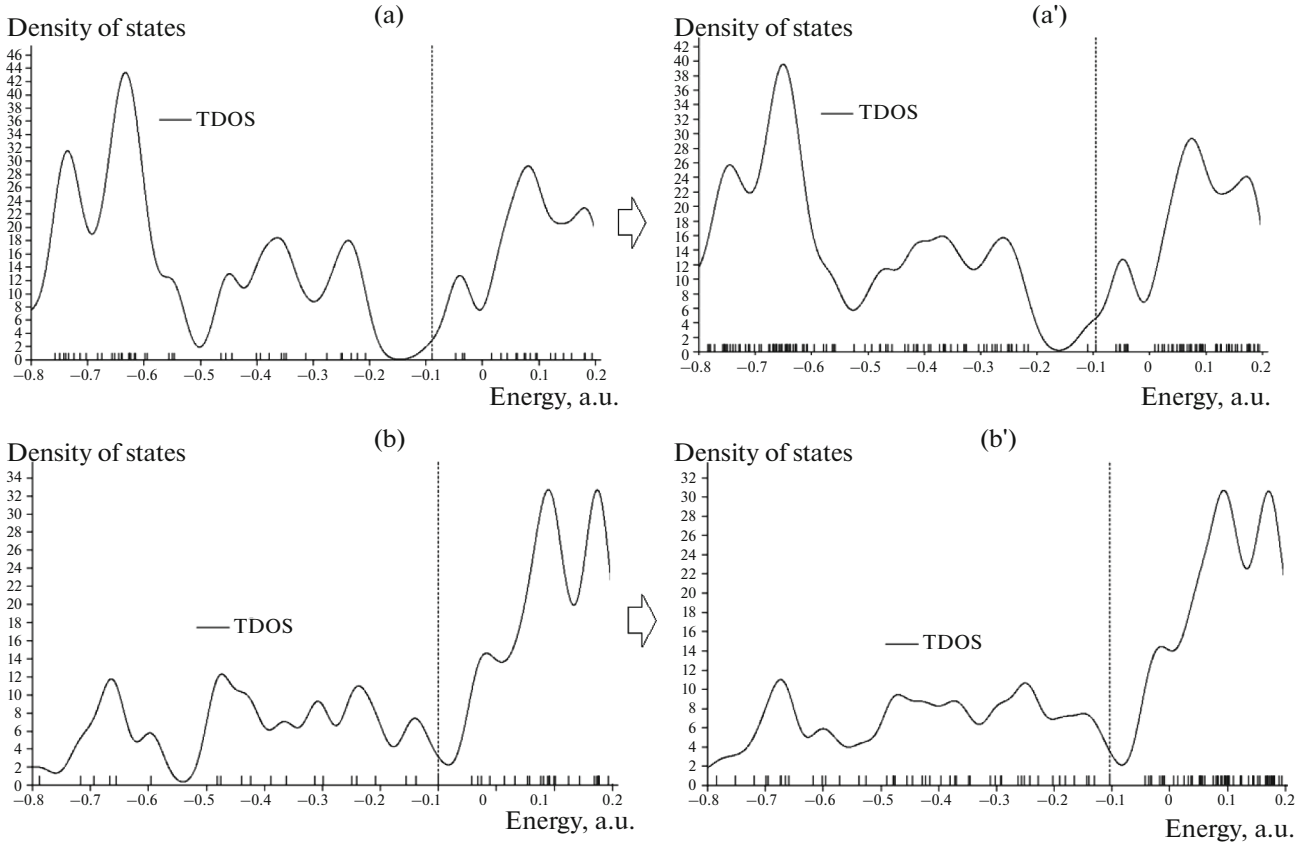

Fig. 4. TDOS graphs of heteroclusters of (a) ZnO, (a') $ZnO(H_2O)$, (b) ZnS, and (b') $ZnS(H_2O)$.

Table 2. LUMO, HOMO, and energy gap (ΔE) for ZnO and ZnS through H/OH adsorption and formation of $ZnO(H_2O)$ and $ZnS(H_2O)$ heteroclusters

Heteroclusters	E_{HOMO}, eV	E_{LUMO}, eV	$\Delta E = E_{LUMO} - E_{HOMO}$, eV
ZnO	−2.43	−1.30	1.12
ZnS	−2.74	−1.17	1.57
$ZnO(H_2O)$	−2.61	−1.60	1.00
$ZnS–H_2O$	−2.74	−1.17	1.67

Table 3. The bond order of Laplacian and Fuzzy, Mayer, Wiberg, and Mulliken from mixed alpha and beta density matrix for ZnO and ZnS through H/OH adsorption and formation of $ZnO(H_2O)$ and $ZnS(H_2O)$ heteroclusters

Bond order	$ZnO(H_2O)$			$ZnS(H_2O)$		
	O1–Zn15	O1–H29	O27–H30	O1–Zn15	O1–H29	S27–H30
Laplacian	1.64	0.21	0.15	1.74	0.20	0.25
Fuzzy	1.65	0.69	0.43	1.52	0.62	0.68
Mayer	1.13	0.65	0.48	1.28	0.69	0.80
Wiberg	1.71	0.66	0.45	1.05	0.64	0.64
Mulliken	1.91	0.17	0.05	1.87	0.15	0.18

$$V_{tot}(r) = V_{nuc}(r) + V_{ele}(r) = \sum_A \frac{Z_A}{|r - R_A|} - \int \frac{\rho(r')}{|r - r'|} dr', \quad (5)$$

Z_A is nuclear charge, if pseudopotential is used, then Z_A is the number of explicitly expressed electrons. Notice that evaluating ESP is much more time-consuming than evaluating other functions. Also note that ESP in Multiwfn is evaluated exactly by nuclear attractive integrals rather than using approximate methods (such as multipole expansion, numerical Poisson equation), hence you may find the results generated by Multiwfn are somewhat different from those outputted by other quantum chemistry codes. In order to speed up ESP evaluation, Multiwfn ignores some integrals that have little contributions. The threshold for ignoring is controlled by "espprecutoff" in settings.ini, enlarging this parameter results in more accurate ESP value, but also brings more computational cost. The ESP evaluated under default value is accurate enough in general cases.

The heteroclusters of $ZnO/ZnO(H_2O)$ and $ZnS/ZnS(H_2O)$ can be defined by ESP graphs owing to exploring their delocalization/localization characterizations of electrons and chemical bonds (Figs. 5a, 5a', 5b, 5b'). Covalent zones have high ESP value, the electron depletion zones between valence shell and inner shell are indicated by the blue circles around nuclei (Figs. 5a, 5a', 5b, 5b'). The counter map of ESP for $ZnO/ZnO(H_2O)$ (Figs. 5a, 5a') and $ZnS/ZnS(H_2O)$ (Figs. 5b, 5b') has shown the localized orbital locator through H/OH adsorption. $ZnO(H_2O)$ or $ZnS(H_2O)$ heterocluster indicates a larger isosurface map of the localized orbital locator due to atoms of O1, Zn15, O27 or S27, H29, H30. A narrower connected area occupied by an isosurface map means that localized orbital locator is relatively difficult. However, the large counter map of ESP for $ZnO(H_2O)$ or $ZnS(H_2O)$ can confirm that ZnO or ZnS can be a promising semiconductor material for various applications.

Moreover, intermolecular orbital overlap integral is important in discussions of intermolecular charge transfer which can calculate HOMO-HOMO and LUMO-LUMO overlap integrals between the H/OH and heterocluster of ZnO or ZnS. The applied wavefunction level is CAM–B3LYP–D3/6–311+G (*d*, *p*) that correspond to HOMO and LUMO, respectively (Table 2). The amount of Mayer bond order [61] is generally according to empirical bond order for the single bond is nearly 1.0. Mulliken bond order [62] with a small accord with empirical bond order is not appropriate for quantifying bonding strength, for which Mayer bond order always performs better. However, Mulliken bond order is a good qualitative indicator for positive amount of bonding and negative amount of antibonding which are evacuated and localized, respectively (Table 3). As it is seen in Table 3, Laplacian bond order [63] has a straight cohesion with bond polarity, bond dissociation energy and bond vibrational frequency. The low value of Laplacian bond order might demonstrate that it is insensitive to the calculation degree applied for producing electron density. Generally, the value of "Fuzzy bond order" is near Mayer bond order, especially for low-polar bonds, but much more stable with respect to the change in basis-set. Computation of Fuzzy bond order demands running Becke's DFT numerical integration [64–70], owing to which the calculation value is larger

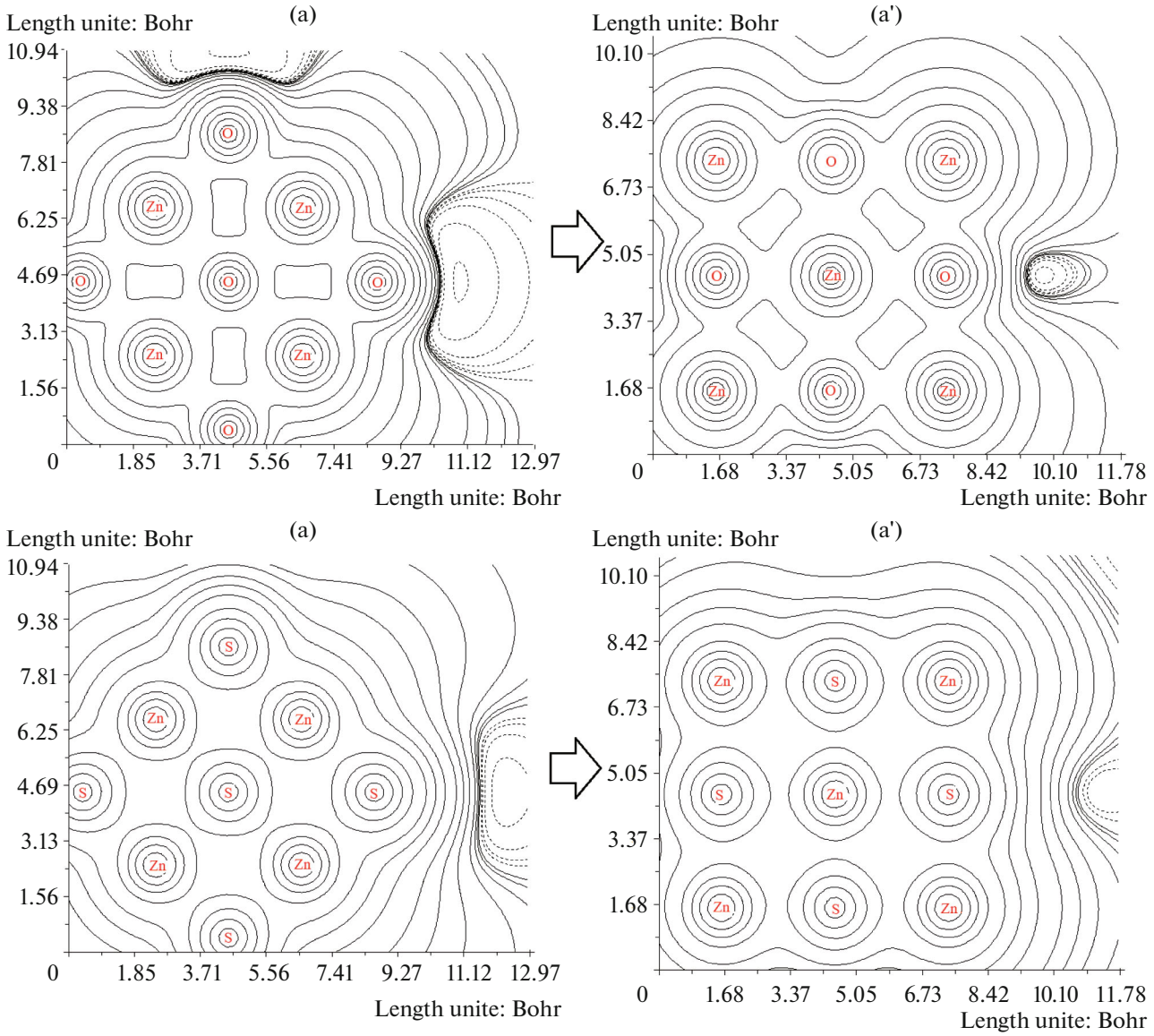

Fig. 5. The counter map of ESP for heteroclusters of (a) ZnO, (a') ZnO(H_2O), (b) ZnS, and (b') ZnS(H_2O).

than assessment of Mayer bond order and it can concede more precisely [71].

4. CONCLUSIONS

ZnO and ZnS have been found to be effective in various strains of microorganisms, and numerous research articles on this area are evidence of its potential as antimicrobial agent. Understanding the interaction of water with ZnO or ZnS is important for this material to be used in gas sensing, catalysis and biomedical applications. In summary, H_2O grabbing on the ZnO or ZnS was investigated by first-principles calculations. We have provided ZnO or ZnS heterocluster, then the geometrical parameters of H/OH adsorption on the surface of ZnO or ZnS through the absorption status and current charge density were studied. ZnO(H_2O) or ZnS(H_2O) heterocluster indicates a larger isosurface map of electron delocalization due to atoms of O1, Zn15, O27 or S27, H29, H30. A narrower connected area occupied by an isosurface map means that electron delocalization is relatively difficult. However, the large counter map of ESP for ZnO(H_2O) or ZnS(H_2O) can confirm that ZnO or ZnS can be a promising semiconductor material for various applications. The challenge is making the use of ZnO and ZnS cost-competitive or incorporating it with conventional water treatment.

ACKNOWLEDGMENTS

In successfully completing this paper and its research, the authors are grateful to Kastamonu University.

FUNDING

This work was supported by ongoing institutional funding. No additional grants to carry out or direct this particular research were obtained.

CONFLICT OF INTEREST

The authors of this work declare that they have no conflicts of interest.

REFERENCES

1. M. A. Borysiewicz, Crystals **9**, 505 (2019). https://doi.org/10.3390/cryst9100505
2. X.Q. Zhang, B. Zhang, Russ. J. Phys. Chem. B **17**, 1049–1056 (2023). https://doi.org/10.1134/S1990793123050135
3. M. I. Ikim, E. Y. Spiridonova, V. F. Gromov, et al., Russ. J. Phys. Chem. B **18**, 283–288 (2024). https://doi.org/10.1134/S199079312401010X
4. A. S. Zverev, A. A. Zvekov, V. M. Pugachev, et al., Russ. J. Phys. Chem. B **17**, 1135–1142 (2023). https://doi.org/10.1134/S1990793123050147
5. X. Yuan, X. Tan, and B. Liu, Russ. J. Phys. Chem. B **17**, 886–895 (2023). https://doi.org/10.1134/S1990793123040322
6. V. Ankam, G. Karka, and L. G. Reddy, Mater. Int. **7**, 1 (2025). https://doi.org/10.33263/Materials71.001
7. S. Parmonov, K. Sharipov, D. Mirzavaliyev, et al., New Mater., Compd. Appl. **8**, 450–458 (2024). https://doi.org/10.62476/nmca83450
8. P. Kirana, C. S. Prashantkumar, R. Soundarya, et al., Mater. Int. **6**, 40 (2024). https://doi.org/10.33263/Materials64.040
9. I. P. Olkhovskaya, I. I. Krokhmal, and N. N. Glushchenko, Russ. J. Phys. Chem. B **18**, 527–532 (2024). https://doi.org/10.1134/S1990793124020295
10. M. Bhat, E. V. Sekhar, and B. K. Sagar, Lett. Appl. NanoBioSci. **14**, 45 (2025). https://doi.org/10.33263/LIANBS141.045
11. N. Kumar, R. Sharma, N. K. Aggarwal, et al., Lett. Appl. NanoBioSci. **13**, 171 (2024). https://doi.org/10.33263/LIANBS134.171
12. H. M. Xiong, D. P. Liu, Y. Y. Xia, et al., Chem. Mater. **17**, 3062–3064 (2005). https://doi.org/10.1021/cm050556r
13. D. C. Agarwal, U. B. Singh, S. Gupta, et al., Sci. Rep. **9**, 6675 (2019). https://doi.org/10.1038/s41598-019-43184-9
14. E. Wolska, J. Kaszewski, P. Kiełbik, et al., Opt. Mater. **36**, 1655–1659 (2014). https://doi.org/10.1016/j.optmat.2013.12.032
15. J. H. Lim, C. K. Kang, K. K. Kim, et al., Adv. Mater. **18**, 2720–2724 (2006). https://doi.org/10.1002/adma.200502633
16. D. B. Tolubayeva, L. V. Gritsenko, Y. Y. Kedruk, et al., Biosensors **13**, 793 (2023). https://doi.org/10.3390/bios13080793
17. H. Liu, Y. Zhang, H. Zhang, et al., J. Transl. Med. **19**, 221(2021). https://doi.org/10.1186/s12967-021-02892-5
18. V. N. Hegde, Lett. Appl. NanoBioSci. **13**, 132 (2024). https://doi.org/10.33263/LIANBS133.132
19. S.-C. Chang, J.-C. Hu, H.-T. Chan, et al., Coatings **12**, 945 (2022). https://doi.org/10.3390/coatings12070945
20. S.-C. Chang, T.-H. Li, and H.-T. Chan, Int. J. Electrochem. Sci. **16**, 210817 (2021). https://doi.org/10.20964/2021.08.34
21. C. Zhang, Z. Cao, G. Zhang, et al., Microchem. J. **158**, 105237 (2020). https://doi.org/10.1016/j.microc.2020.105237
22. S. Nundy, A. Ghosh, and T. K. Mallick, ACS Omega **5**, 1033–1039 (2020). https://doi.org/10.1021/acsomega.9b02758
23. I. S. Yakovenko and A. D. Kiverin, Russ. J. Phys. Chem. B **18**, 1069–1076 (2024). https://doi.org/10.1134/S1990793124700623
24. M. Monajjemi, S. Mohammadi, S. Shahriari, et al., Russ. J. Phys. Chem. B **18**, 308–324 (2024). https://doi.org/10.1134/S1990793124010342
25. S. Z. Zainabidinov, A. Y. Boboev, M. B. Rasulova, et al., New Mater., Compd. Appl. **8**, 411–421 (2024). https://doi.org/10.62476/nmca83411
26. E. A. Yakush, A. V. Kim, and N. N. Medvedev, Russ. J. Phys. Chem. B **18**, 252–257 (2024). https://doi.org/10.1134/S199079312401038X
27. A. A. Vasin, A. L. Dobryakov, S. Y. Kochev, et al., Russ. J. Phys. Chem. B **18**, 1646–1650 (2024). https://doi.org/10.1134/S1990793124701380
28. A. Castro, S. Calderon, and L. Marques, Materials **16**, 1275 (2023). https://doi.org/10.3390/ma16031275
29. G. Wang, B. Huang, Z. Li, et al., Sci. Rep. **5**, 8544 (2015). https://doi.org/10.1038/srep08544
30. A. U. Khan, K. Tahir, K. Albalawi, et al., Mater. Chem. Phys. **291**, 126667 (2022). https://doi.org/10.1016/j.matchemphys.2022.126667
31. D. Zagorac, J. Zagorac, M. Pejić, et al., Nanomaterials **12**, 1595 (2022). https://doi.org/10.3390/nano12091595
32. N. P. de Moraes, L. G. P. Marins, M. Y. de Moura Yamanaka, et al., J. Photochem. Photobiol. A: Chem. **418**, 113377 (2021). https://doi.org/10.1016/j.jphotochem.2021.113377
33. A. Bolatov, A. Manjovelo, B. Chouchene, et al., Materials **17**, 4877 (2024). https://doi.org/10.3390/ma17194877
34. V. Chaudhari, M. Dharmadhikari, and V. Kolhe, Letters in Appl. NanoBioSci. **13**, 80 (2024). https://doi.org/10.33263/LIANBS132.080
35. F. Mollaamin and M. Monajjemi, New Mater., Compd. Appl. **8**, 303–323 (2024). https://doi.org/10.62476/nmca83303
36. F. Mollaamin, Russ. J. Phys. Chem. B **18**, 805–820 (2024). https://doi.org/10.1134/S1990793124700131
37. F. Mollaamin, S. Shahriari, M. Monajjemi, et al., J. Cluster Sci. **34**, 1547–1562 (2023). https://doi.org/10.1007/s10876-022-02335-1
38. M. Monajjemi, N. Karachi, and F. Mollaamin, Fullerenes Nanotubes Carbon Nanostruct. **22**, 643–662 (2014). https://doi.org/10.1080/1536383X.2012.717557

39. F. Mollaamin and M. Monajjemi, J. Mol. Model. **29**, 119 (2023). https://doi.org/10.1007/s00894-023-05526-3
40. F. Mollaamin and M. Monajjemi, Russ. J. Phys. Chem. B 18, 1177–1198 (2024). https://doi.org/10.1134/S1990793124700507
41. F. Mollaamin and M. Monajjemi, J. Mol. Model. **29**, 170 (2023). https://doi.org/10.1007/s00894-023-05567-8
42. M. Monajjemi, H. Yamola, and F. Mollaamin, Fullerenes Nanotubes Carbon Nanostruct. **22**, 595–603 (2014). https://doi.org/10.1080/1536383X.2012.702163
43. F. Mollaamin and M. Monajjemi, J. Cluster Sci. **34**, 2901–2918 (2023). https://doi.org/10.1007/s10876-023-02436-5
44. F. Mollaamin and M. Monajjemi, Russ. J. Phys. Chem. B **17**, 658–672 (2023). https://doi.org/10.1134/S1990793123030223
45. F. Mollaamin and M. Monajjemi, C—J. Carbon Res. **9**, 20 (2023). https://doi.org/10.3390/c9010020
46. F. Mollaamin and M. Monajjemi, Int. J. Quantum Chem. **124**, e27348 (2024). https://doi.org/10.1002/qua.27348
47. F. Mollaamin and M. Monajjemi, Mol. Simul. **49**, 365–376 (2023). https://doi.org/10.1080/08927022.2022.2159996
48. F. Mollaamin and M. Monajjemi, Sensor Rev. **43**, 266–279 (2023). https://doi.org/10.1108/SR-03-2023-0040
49. M. J. Frisch, G. W. Trucks, H. B. Schlegel, G. E. Scuseria, M. A. Robb, J. R. Cheeseman, G. Scalmani, V. Barone, G. A. Petersson, H. Nakatsuji, X. Li, M. Caricato, A. V. Marenich, J. Bloino, B. G. Janesko, R. Gomperts, B. Mennucci, H. P. Hratchian, J. V. Ortiz, A. F. Izmaylov, J. L. Sonnenberg, D. Williams-Young, F. Ding, F. Lipparini, F. Egidi, J. Goings, B. Peng, A. Petrone, T. Henderson, D. Ranasinghe, V. G. Zakrzewski, J. Gao, N. Rega, G. Zheng, W. Liang, M. Hada, M. Ehara, K. Toyota, R. Fukuda, J. Hasegawa, M. Ishida, T. Nakajima, Y. Honda, O. Kitao, H. Nakai, T. Vreven, K. Throssell, J. A. Montgomery, Jr., J. E. Peralta, F. Ogliaro, M. J. Bearpark, J. J. Heyd, E. N. Brothers, K. N. Kudin, V. N. Staroverov, T. A. Keith, R. Kobayashi, J. Normand, K. Raghavachari, A. P. Rendell, J. C. Burant, S. S. Iyengar, J. Tomasi, M. Cossi, J. M. Millam, M. Klene, C. Adamo, R. Cammi, J. W. Ochterski, R. L. Martin, K. Morokuma, O. Farkas, J. B. Foresman, and D. J. Fox, *Gaussian 16, Revision C.01* (Gaussian, Inc., Wallingford, CT, 2016).
50. R. Dennington, T. A. Keith, and J. M. Millam, *GaussView, Version 6.06.16* (Semichem Inc., Shawnee Mission, KS, 2016).
51. T. Yanai, D. P. Tew, and N. C. Handy, Chem. Phys. Lett. **393**, 51–57 (2004). https://doi.org/10.1016/j.cplett.2004.06.011
52. S. Grimme, S. Ehrlich, and L. Goerigk, J. Comput. Chem. **32**, 1456–1465 (2011). https://doi.org/10.1002/jcc.21759
53. Z. Xu, C. Qin, Y. Yu, et al., AIP Adv. **14**, 055114 (2024). https://doi.org/10.1063/5.0208082
54. F. Mollaamin and M. Monajjemi, Adv. Phys. Res. **7**, 5–28 (2025). https://doi.org/10.62476/apr.7105
55. T. Lu and F. Chen, J. Comput. Chem. **33**, 580–592 (2012). https://doi.org/10.1002/jcc.22885
56. T. Lu, J. Chem. Phys. **161**, 082503 (2024). https://doi.org/10.1063/5.0216272
57. A. H. Davtyan, Z. O. Manukyan, S. D. Arsentev, et al., Russ. J. Phys. Chem. B **17**, 336–345 (2023). https://doi.org/10.1134/S1990793123020239
58. J. S. Murray, P. Politzer, Comput. Mol. Sci. **1**, 153–163 (2011). https://doi.org/10.1002/wcms.19
59. R. Lopez, F. Martinez, I. Ema, et al., Computation **7**, 64 (2019). https://doi.org/10.3390/computation7040064
60. J. S. Murray, K. E. Riley, and T. Brinck, Crystals **14**, 995 (2024). https://doi.org/10.3390/cryst14110995
61. I. Mayer, Chem. Phys. Lett. **544**, 83–86 (2012). https://doi.org/10.1016/j.cplett.2012.07.0
62. F. Mollaamin and M. Monajjemi, J. Fluoresc. (2025). https://doi.org/10.1007/s10895-025-04207-z
63. T. Lu and F. Chen, J. Phys. Chem. A **117**, 3100–3108 (2013). https://doi.org/10.1021/jp4010345
64. V. B. Orel and A. A. Manzhueva, Russ. J. Phys. Chem. B **17**, 835–844 (2023). https://doi.org/10.1134/S1990793123040152
65. H. Touhami, K. Almi, S. Lakel, et al., Russ. J. Phys. Chem. B **17**, 1057–1068 (2023). https://doi.org/10.1134/S1990793123050287
66. F. Mollaamin, S. Mohammadi, Z. Khalaj, et al., Russ. J. Phys. Chem. B **18**, 67–82 (2024). https://doi.org/10.1134/S1990793124010330
67. V. D. Makhaev, L. A. Petrova, G. V. Shilov, et al., Russ. J. Phys. Chem. B **18**, 388–397 (2024). https://doi.org/10.1134/S1990793124020258
68. Y. A. Dyakov, S. O. Adamson, N. I. Butkovskaya, et al., Russ. J. Phys. Chem. B **18**, 682–691 (2024). https://doi.org/10.1134/S1990793124700179
69. V. E. Zobov and A. A. Lundin, Russ. J. Phys. Chem. B **18**, 1249–1262 (2024). https://doi.org/10.1134/S1990793124701070
70. D. R. Diniakhmetova and S. V. Kolesov, Russ. J. Phys. Chem. B **18**, 1478–1485 (2024). https://doi.org/10.1134/S1990793124701410
71. X. Wang, X. Zhang, W. Pedrycz, et al., Fractal Fract. **8**, 523 (2024). https://doi.org/10.3390/fractalfract8090523